Mine Water and the Environment (2020) 39:699–715
https://doi.org/10.1007/s10230-020-00695-6

TECHNICAL ARTICLE

Using Statistical and Dynamical Downscaling to Assess Climate Change Impacts on Mine Reclamation Cover Water Balances

Md. Shahabul Alam[1] · S. Lee Barbour[1,2] · Mingbin Huang[1,4] · Yanping Li[2,3]

Received: 9 February 2020 / Accepted: 8 June 2020 / Published online: 14 June 2020

Abstract

The oil sands industry in Canada uses soil–vegetation–atmosphere-transfer (SVAT) water balance models, calibrated against short-term (<≈ 10 years) field monitoring data, to evaluate long-term (≈60 years) reclamation cover design performance. These evaluations use long-term historical climate data; however, the effects of climate change should also be incorporated in these analyses. Although statistical downscaling of global climate change projections is commonly used to obtain local, site-specific climate, high resolution dynamical downscaling can also be used. The value of this latter approach to obtain local site-specific projections for mine reclamation covers has not been evaluated previously. This study explored the differences in key water balance components of three reclamation covers and three natural sites in northern Alberta, Canada, under future, site-specific, statistical, and dynamical climate change projections. Historical meteorological records were used to establish baseline periods. Temperature datasets were used to calculate potential evapotranspiration (PET) using the Hargreaves–Samani method. Statistical downscaling uses the Long Ashton Research Station Weather Generator (LARS-WG) and global circulation model (GCM) projections of temperature and precipitation. Dynamical climate change projections were generated on a 4 km grid using the weather research and forecasting (WRF) model. These climate projections were applied to a physically-based water balance model (i.e. Hydrus-1D) to simulate actual evapotranspiration (AET) and net percolation (NP) for the baseline and future periods. The key findings were: (a) LARS-WG outperformed WRF in simulating baseline temperatures and precipitation; (b) both downscaling methods showed similar directional shifts in the future temperatures and precipitation; (c) this, in turn, created similar directional shifts in future growing season median AET and NP, although the increase in future NP for LARS-WG was higher than that for WRF. The relative increases in future NP were much higher than the relative increases in future AET, particularly for the reclamation covers.

Keywords Future climate · LARS-WG · WRF · Water balance model · Evapotranspiration · Net percolation

Introduction

Oil sands represent 98% of Canada's proven oil reserves and the extraction and mining of oil sands in northern Alberta plays an important role in Canada's economy. Total oil production in 2018 was 4.59 million barrels per day and is expected to reach 5.86 million barrels per day by the end of 2035 (CAPP 2019). The oil sands underlie ≈ 140,000 km^2 in northern Alberta, Canada, where shallow (up to 75 m depth) mineable reserves comprise an area of ≈ 4800 km^2, of which more than 895 km^2 (18% of the total shallow mineable area) has been disturbed or cleared in association with surface mining activities (Government of Alberta 2017). The oil sands industries are obliged by law to reclaim the land to an equivalent land capability after oil sands have been extracted (CEMA 2006).

Electronic supplementary material The online version of this article (https://doi.org/10.1007/s10230-020-00695-6) contains supplementary material, which is available to authorized users.

✉ Md. Shahabul Alam
msa181@usask.ca

[1] Deparment of Civil, Geological and Environmental Engineering, University of Saskatchewan, Saskatoon, SK S7N 5A9, Canada

[2] Global Institute for Water Security, University of Saskatchewan, Saskatoon, SK S7N 3H5, Canada

[3] School of Environment and Sustainability, University of Saskatchewan, Saskatoon, SK S7N 5C8, Canada

[4] Center for Excellence in Quaternary Science and Global Change, Chinese Academy of Sciences, Xian 710061, China

The design of reclamation covers is currently based on the use of soil–vegetation–atmosphere-transfer (SVAT) water balance models calibrated against relatively short-term ($< \approx 10$ years) monitoring undertaken on prototype covers. These calibrated models are then used along with long-term (≈ 60 years) historical climate records to simulate future cover performance (Boese 2003; Huang et al. 2011a, b, c, 2015a; Keshta et al. 2009; Price et al. 2010; Qualizza et al. 2004). There is a growing appreciation by industry that this design approach must begin to incorporate the potential impacts of climate change.

Historical climate records have indicated that temperature and precipitation are increasing globally (e.g. Alexander et al. 2006; IPCC 2013; Zhang et al. 2000) with more frequent extreme weather (e.g. drought, flooding, and heatwaves; Chen 2013; Held and Soden 2006; Karl et al. 1995; Li et al. 2017; Liu et al. 2017; Sun 2014; Wood et al. 1997). In Canada, there has been a 0.3 °C increase in annual mean temperature and a 5–35% increase in annual precipitation from 1950 to 1998 (Zhang et al. 2000). The twenty-first century climate change projections indicate precipitation increases across Canada including the Canadian prairies (e.g. Alam and Elshorbagy 2015; Hassanzadeh et al. 2014; Srivastav et al. 2014; Suncor Energy Inc. 2007; Thompson et al. 2017).

The primary tool for future climate projections has been the general circulation models (GCMs; Meehl et al. 2007). These projections play a vital role in studying the impacts of climate change and variability (Fowler et al. 2007). The GCM projections have been coordinated and distributed by the coupled model intercomparison project (CMIP) with support from the world climate research programme's (WCRP) working group on coupled modelling (WGCM). Since program inception, five different phases of multi-model research activity (Meehl et al. 2004, 2007; Taylor et al. 2012) have been published; these form the central basis of national and international studies of climate change (IPCC 2013).

GCMs have coarse spatial resolutions (typically 100–300 km), which limit their value in predicting local (site specific) and regional (typically 25–50 km) climate change characteristics since convective cloud processes (a primary producer of precipitation) are not represented adequately at these scales (Joubert and Hewitson 1997). The most commonly used methods of downscaling GCMs to local and regional scales has been through statistical or dynamical downscaling techniques (Fowler et al. 2007; Wilby and Wigley 1997). Both approaches have certain advantages and disadvantages. For example, while statistical downscaling is computationally efficient, dynamic downscaling is able to produce high resolution climate variables based on physical processes (Fowler et al. 2007; Wilby and Dawson 2007). Since northern Alberta is located in the Canadian Prairies, the precipitation in this region is mostly contributed by summer convection; consequently, any downscaling method must capture these convection-driven effects.

Statistical downscaling is based on the statistical relationships between the local-scale climate variables (the predictands) and the global-scale climate variables (the predictors) to generate site-specific climate change projections (Wilby et al. 1998). Statistical downscaling approaches developed over the past 20–30 years include both simple methods (e.g. delta change) and more sophisticated methods (e.g. regression models, stochastic weather generators, weather typing schemes). Each of these methods are based on a range of theories; however, all of them rely on the fundamental relationship established between large-scale atmospheric condition and local-scale features (Fowler et al. 2007). In practice, two or more approaches can be combined and therefore, many approaches are a hybrid of the basic methods (Wilby and Wigley 1997).

A potential improvement in downscaling has been the use of dynamical downscaling by parameterizing physical atmospheric processes. In a dynamical downscaling approach, finer resolution information from GCM-based outputs is generated by embedding a high-resolution regional climate model (RCM) within a GCM (Fowler et al. 2007; Wilby and Dawson 2007). The high resolution projections explicitly account for underlying surface and local circulation patterns to represent several small-scale characteristics and atmospheric processes that cannot be captured using GCMs (Castro et al. 2005; Gao et al. 2012; May 2008).

RCMs can provide more resolution of small-scale processes than the GCMs; however, RCMs are still at a relatively coarse resolution where convection-dominated precipitation is poorly represented. A high-resolution weather forecasting model with convection-permitting scheme known as weather research and forecasting (WRF; Skamarock et al. 2008) model incorporates horizontal grid spacing of less than 4 km. At this grid spacing, WRF begins to reflect the impact of convective processes, as influenced by underlying surface topography (Li et al. 2019). Despite its higher computational costs, high resolution WRF has demonstrated benefits when used in dynamical downscaling (Done et al. 2004; Fosser et al. 2015; Prein et al. 2017; Weisman et al. 2008). WRF simulations also add value to the study of climate change impacts in regions such as western Canada where small-scale atmospheric processes (e.g. summer convections) are important (Li et al. 2017, 2019).

However, the outputs of WRF (as well as the outputs of any RCM) are impacted by a series of procedures connected to climate model uncertainties due to nested modelling. The series of uncertainties (termed as a cascade of uncertainty by Mitchell and Hulme 1999) has impact on the outcomes of the subsequent levels. For example, GCMs outputs are impacted by the uncertainties in the

assumption of emission scenarios, while the WRF outputs are impacted by the uncertainties in the simulations of the driving GCMs. These uncertainties are propagated from emission scenarios to GCMs toward WRF outputs with increasing magnitude. It is important to note that these uncertainties are accounted for in the end projections of climate change, where these uncertainties are recognized as inevitable in the process of climate modelling (Foley 2010).

The key components of the water balance for the design of reclamation soil covers are the actual evapotranspiration (AET), reflective of vegetative growth, and net percolation (NP), reflective of the contribution to groundwater flow through the underlying mining waste, which may transport chemical constituents from these deposits. Previous studies have shown that increases in future temperature will result in increases in both AET and NP. Alam et al. (2017) incorporated climate change projections from three GCMs (e.g. CanESM2, BCC-CSM1.1, and IPSL-CM5A-LR) based on three representative concentration pathways (RCP2.6, RCP4.5, and RCP8.5) into a physically-based water balance model (i.e. Hydrus-1D) to quantify uncertainties in the projected AET and NP of an oil sands reclamation cover and a natural soil profile. Alam et al. (2018) used a similar framework to quantify uncertainties in the projected AET and NP of two reclamation covers and three natural soil profiles using the fourth generation Canadian GCM (CanESM2), based on the three RCPs.

Keshta et al. (2012) studied reclamation cover water balances using a generic system dynamics water balance model in which they incorporated climate change projections. The projections were taken from the third generation Canadian GCM (i.e. CGCM3) based on two scenarios from the special report on emission scenarios (SRES); emission scenarios (A2 and B1, IPCC 2000). Their study showed that decreases in soil moisture deficit and increases in AET are associated with the projected increases in precipitation. They did not evaluate potential changes in NP.

High-resolution WRFs or RCMs have not been previously used to evaluate the future water balance performance of mine reclamation soil covers. The overall objective of this study was to evaluate the relative impact of using statistically and dynamically downscaled climate change projections from the GCMs on predictions of the future water balance performance of three reclamation soil covers and three natural vegetation sites in northern Alberta, Canada. These predictions were undertaken in a manner to also quantify the uncertainties in the projected AET and NP of the oil sands reclamation covers and natural soil profiles for each of the downscaling methods.

Materials and Methods

Study Sites, Reclamation Covers, and Natural Sites

The study area is situated within the boreal mixed-wood ecoregion (Strong and Leggat 1981), ≈40–80 km north of Fort McMurray, Alberta, Canada. The climate is a typical prairie climate with an average annual precipitation of 427 mm (1944–2018), approximately two-thirds of which occurs in the summer months. The mean spring (March–May), summer (June–August), fall (September–November), and winter (December–February) temperatures are 2.0, 15.5, 5.7, and − 15.2 °C, respectively. The average annual potential evapotranspiration (PET) in Fort McMurray is 670 mm, based on the Hargreaves-Samani method and meteorological observations from the Fort McMurray Airport station over a 75-year period (1944–2018).

This study focuses on three reclamation soil cover sites [South Bison Hill (D3), Southwest Sand Tailings Storage (SWSS), Aurora Capping Study (ACS)] as well as three monitored natural soil profiles (soil vegetation sites SV10, SV27, and SV60) located at undisturbed reference sites (Fig. 1). Two of the reclamation covers (D3 and SWSS) are located at Syncrude Canada Ltd's (SCL) Mildred Lake mine site, while the ACS reclamation cover is located at the SCL Aurora North mine, ≈20 km to the north of the Mildred Lake Mine. The D3 and ACS prototype covers are ≈1 hectare in size but sit within much larger areas (several hundred hectares) of reclaimed mine waste.

The reclamation soil profiles at each site are:

- D3 site: 20 cm of a salvaged peat-glacial clay mineral mixture overlying 80 cm of a glacial clay soil overlying shale overburden;
- SWSS: 45 cm of peat-glacial clay mineral mixture overlying tailings sand;
- ACS: 20 cm of cover soil (either salvaged peat or upland surface litter layer) overlying 100 cm of salvaged sandy subsoil placed over lean oil sands (LOS) overburden.

The reclamation covers have been monitored since 1999 (D3), 2001 (SWSS), and 2012 (ACS). The monitoring includes meteorology (precipitation, air temperature, wind speed, net radiation, and relative humidity), as well as soil monitoring (volumetric water content, suction, and soil temperature) across the cover profile and into the underlying mine waste. Details of the instrumentation and monitoring program can be found in Barbour et al. (2004), Boese (2003), Huang et al. (2015a), O'Kane Consultants Inc. (OKC 2001, 2016).

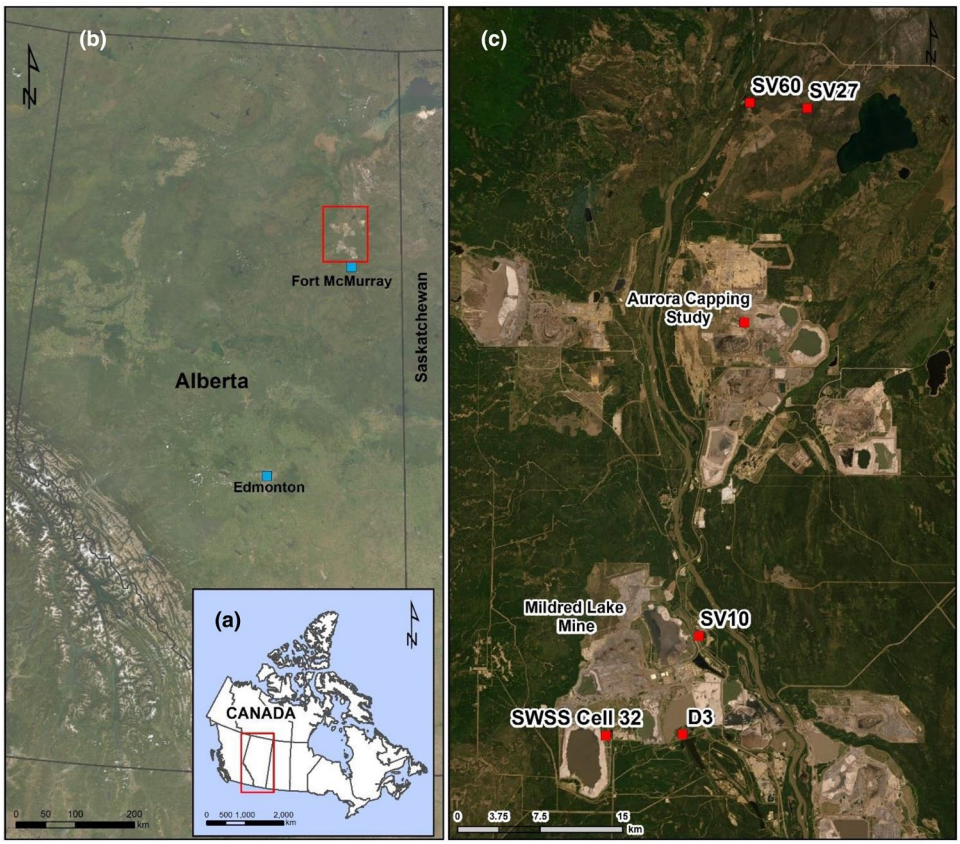

Fig. 1 **a** Map of Canada showing the province of Alberta, **b** map of Alberta showing the relevant cities and general study area, and **c** map of the study area showing the site locations with red squares where **c** is the zoom out view of the red rectangle in (**b**). Map sources: Esri, DigitalGlobe, GeoEye, Earthstar, Geographics, CNES/Airbus DS, USDA, USGS, Aerogrid, IGN, and the GIS User Community

The monitored natural soil profile locations follow: SV10 is at the Mildred Lake Mine site and SV27 and SV60 are ≈20 km north of the ACS reclamation cover site. The SV10 and SV27 sites are texturally homogeneous with fine or medium sands, respectively. SV60 is texturally heterogeneous with a fine sand layer (45–84 cm) overlain and underlain by coarse sand layers. The details of these sites, including field experiments and measurements of soil properties, can be found in Huang et al. (2011b) and Zettl et al. (2011).

Data Collection

The reference historical data set for the region was a 60 year (1956–2015) daily climate monitoring record obtained from Environment and climate change Canada (ECCC) records at the Fort McMurray Airport station (syncrude.emline.ca/Syncrude/Pages/default.aspx). The global scale future climate change projections (i.e. precipitation and temperature) for the historical period (1976–2005) and future period (2086–2100) were obtained from the CMIP5 GCMs (see the list in supplemental Table S-1), based on the representative concentration pathways (RCP8.5). The climate change projections were obtained from the CMIP5 data archive (https://esgf-node.llnl.gov/search/cmip5/). The WRF-simulated climate change projections (i.e. hourly precipitation and temperature) for the baseline (2001–2015) and future (2086–2100) periods were obtained through dynamical downscaling from Li et al. (2017, 2019). All the climate change projections were obtained for the Fort McMurray Airport station (56.6488° N, 111.2305° W).

Downscaling Methods

Two approaches to downscaling were used in this study. The first was statistical downscaling of GCM projections using the Long Ashton Research Station Weather Generator (LARS-WG) and the second was dynamical downscaling based on WRF simulations.

The high computational demands of the WRF model (≈2 years run time using Compute Canada's resources) required that this study rely on currently available simulation time periods. This included 15 years of simulation results for the 2001–2015 historical period and the 2086–2100 future period. This was further constrained by the long-term historical and future time horizons for the GCMs used for the LARS-WG downscaling. These time horizons were 1976–2005 and 2086–2100, respectively. These differing historical and future time periods for the two downscaling methods were unavoidable and complicate the inter-comparisons. As a result, the inter-comparisons between the LARS-WG and WRF models was only possible for the shorter period of overlap (2001–2005).

Statistical Downscaling

The statistical downscaling method in this study was the latest version of LARS-WG 5.5 (Racsko et al. 1991; Semenov 2007; Semenov and Barrow 1997). The stochastic weather generator LARS-WG can generate synthetic weather time-series (e.g. daily precipitation, and daily minimum and maximum temperatures) for any duration. LARS-WG computes a set of parameters for the distributions of observed climate variables as well as correlations between different observed daily climate variables. Synthetic time series of climate variables are generated using the set of parameters by randomly selecting values from the appropriate distributions. These selected parameter distributions for a given site are then perturbed by the relative changes as projected by the GCMs (i.e. climate scenario) to generate a future climate scenario for the site.

Future climate scenarios were calculated using the synthetic monthly distributions from historic GCM projections, adjusted to align with historical distributions of these variables, and then perturbed based on the GCM projections of future climate change. In this study, the climate scenarios for LARS-WG simulations were derived from the CMIP5 multi-model ensemble based on the mean of 17 member GCMs for RCP8.5 scenario during the future period 2086–2100 relative to the historical period 1976–2005. The list of the member GCMs from CMIP5 used in LARS-WG simulations are shown in supplemental Table S-1.

Dynamical Downscaling

The WRF model was used to simulate the regional climate for the historical baseline and future climate with reanalysis and climate change forcing based on the ensembles of CMIP5 GCMs (RCP8.5), respectively. The dynamical downscaling technique relied on simulations undertaken by Li et al. (2017, 2019) using the WRF version 3.6.1 model (Skamarock et al. 2008). This WRF model simulated historical (2001–2015) climate and dynamically downscaled projected climate for a future period (2086–2100) over a domain covering western Canada from British Columbia to the Yukon. The WRF model domain was composed of 700×640 grid points with a horizontal resolution of 4 km.

The WRF simulations included an initial simulation [control experiment (CTL)] of the historical baseline climate by directly forcing 6 h 0.7° ERA-Interim reanalysis data (Dee et al. 2011). A second simulation, based on a climate perturbation of sensitivity experiment [pseudo-global warming (PGW); Rasmussen et al. 2011, 2014)], was used to simulate future climate change projections using the PGW forcing derived from climate change signals from a 19-member ensemble mean of CMIP5 GCMs, as recommended by Liu et al. (2017). The PGW simulation for a 15 year period (2086–2100) was forced with the same ERA-interim reanalysis as in CTL, plus a climate perturbation based on ensemble of CMIP5 RCP8.5 projections:

$$\mathrm{PGW-forcing} = \mathrm{ERA-Interim} + \Delta_{CMIP5\_RCP8.5}$$

where $\Delta_{CMIP5\_RCP8.5}$ is the climate change signals derived from the CMIP5 multi-model ensemble based on the mean of 19 member GCMs for RCP8.5 scenario during the future period 2071–2100 relative to the historical period 1976–2005. For more details on WRF simulations, please refer to Li et al. (2017, 2019). The list of these member GCMs from CMIP5 used in WRF simulations are shown in supplemental Table S-1.

Water Balance Modelling

The physically-based soil water dynamics model, Hydrus-1D (Simunek et al. 2013), was used to simulate key water balance components (AET and NP) for each of the study sites. This modelling approach has been used extensively to study long-term water balance, soil water dynamics, and alternative reclamation cover designs for oil sands reclamation covers (e.g. Huang et al. 2011a, b, c, 2015a, b; Sigouin et al. 2016; Zettl et al. 2011).

The model is based on the solution of Richard's equation for transient water flow through unsaturated soil including soil-atmosphere transfers (i.e. evaporation and transpiration) using the method proposed by Feddes et al. (1974). In this method, actual evaporation and actual transpiration are calculated based on prescribed vegetation characteristics, such as leaf area index (LAI) and root length density. Details of the models including the material properties, the vegetation (i.e. LAI), and root densities were presented in previous papers (Alam et al. 2017, 2018; Huang et al. 2011b, c, 2015a). Typical particle size distributions, water retention curves (WRCs), and distributions of saturated hydraulic conductivity (Ks) are shown in supplemental Figs. S-1, S-2, and S-3).

The Hydrus-1D model was previously calibrated and validated against field monitoring data at the study sites including: D3 (Huang et al. 2015a), SWSS (Alam et al. 2018), ACS (Alam et al. 2020), and three natural sites (SV10, SV27, and SV60; Huang et al. 2011b, c). The model domains used for each site were:

- D3: three layers (i.e., peat-mineral soil mixture, secondary clay layer, and underlying overburden shale);
- SWSS: two layers (i.e., peat-mineral mixture and tailings sand);
- ACS: three layers (i.e., peat cover soil, coarse-textured subsoil, and lean oil sand substrate);

- Natural profiles: the texturally variable natural sand profiles required 14, 20, and 18 layers of varying texture and bulk density at SV10, SV27, and SV60, respectively.

A lower free drainage (i.e. unit vertical gradient) boundary condition was used in all of the models, consistent with the deep water table at all sites. This allows the surface soil water balance to be decoupled from the deeper hydrogeologic system (Dobchuk et al. 2013).

The simulated growing season precipitation and the calculated PET using Hargreaves-Samani method were used to represent the upper boundary condition in Hydrus-1D model. The Hargreaves equation (Hargreaves and Samani 1985) was used to calculate PET (mm/day), based on the daily temperature values:

$$\mathrm{PET} = 0.0023 R_a \left(T_{mean} + 17.8\right)\left(T_{max} - T_{min}\right)^{0.5}$$

where: Ra = water equivalent of extraterrestrial radiation (mm/day); T_{mean} = mean daily air temperature (°C); T_{max} = mean daily maximum air temperature (°C); and T_{min} = mean daily minimum air temperature (°C). The calculated daily PET during the growing season was applied as input in the water balance model.

The daily precipitation during the winter (typically November–March) from both WRF and LARS-WG were accumulated within a snowpack if the mean temperature in a day was less than 0 °C. The accumulated snowpack was then released into the soil domain over an assumed 2-week snowmelt period (typically in the first 2 weeks of April). The volume of snowpack melt over the winter period was calculated when the mean temperature in a day exceeded 0 °C using the degree-day method as outlined by Carrera-Hernandez et al. (2011). A similar approach was used by Alam et al. (2018). The details are not repeated here for brevity. In brief, the calculated volume of melted snowpack was added to the precipitation amounts that occurred during the winter melt period and to any stored profile water within the soil profile at the beginning of the growing season.

The near surface hydraulic conductivity at all the sites was higher than that of the underlying soil layers (i.e. $> 1 \times 10^{-06}$ m/s or 86 mm/day). The cover soils typically have a hydraulic conductivity $> 1 \times 10^{-06}$ m/s, while the underlying soils have a typical hydraulic conductivity of $< 1 \times 10^{-06}$ m/s. The reclamation covers were constructed with an average slope less than 10%, while the natural soil vegetation sites were flat. The higher surface hydraulic conductivity and the flat-lying topography (Alam et al. 2018; Bockstette 2018; Huang et al. 2011b; Meiers et al. 2011) enabled us to simplify the models by assuming there was no runoff. Infiltrated water in excess of available storage reports as net percolation, which now defines the total water release (i.e. water yield) from the reclamation covers.

Results and Discussion

The simulated climate change projections from the two downscaling methods (WRF and LARS-WG) are compared with historic observational data as well as for future time periods. The climate projections from both downscaling methods are also applied to the physically-based model to simulate both historic and future key water balance components (i.e. AET and NP) for three reclamation covers and three natural soil profiles.

Downscaled Climate Change Projections

Comparison of LARS-WG and WRF Models with Historical Observations

The range of daily temperatures (Tmin, Tmax, and Tmean) and total precipitation each month from the LARS-WG and WRF-CTL simulations are compared with observations from the Fort McMurray Airport Station in Fig. 2.

The LARS-WG reproduces the overall seasonal variations in precipitation and temperature (i.e. Tmin, Tmax, and Tmean) reasonably well with relatively small over- or under-estimates of precipitation and temperature in some months. In this study, the overall performance of LARS-WG was acceptable with relative errors of less than 10% between the observed and simulated median precipitation and temperature values in most months. Similar results were obtained in previous studies (e.g. Alam and Elshorbagy 2015; Alam et al. 2018; Chun et al. 2013; Nazemi et al. 2011).

WRF is able to reproduce the mid-summer through fall monthly temperature variability with similar peak values of temperature and precipitation occurring in July, consistent with the observed dataset. The simulated temperatures were lower in all months, while the WRF-simulated precipitation was higher in most months than the observed dataset. The overall relative error was 69.5% between the observed and simulated median precipitation and temperature values, considering all months.

Both downscaling models were better able to replicate the observed variability of precipitation than that of temperature in most months. The WRF-simulated temperature and precipitation were systematically under- and over-estimated, respectively, for most months, while LARS-WG outperformed WRF (Fig. 2). The underestimated temperature was due to the cold biases (particularly between March and July), while the overestimated precipitation was due to the wet biases for all seasons and more pronounced biases in the extreme precipitation amounts, as explained by Li et al. (2019). The July simulated values from WRF,

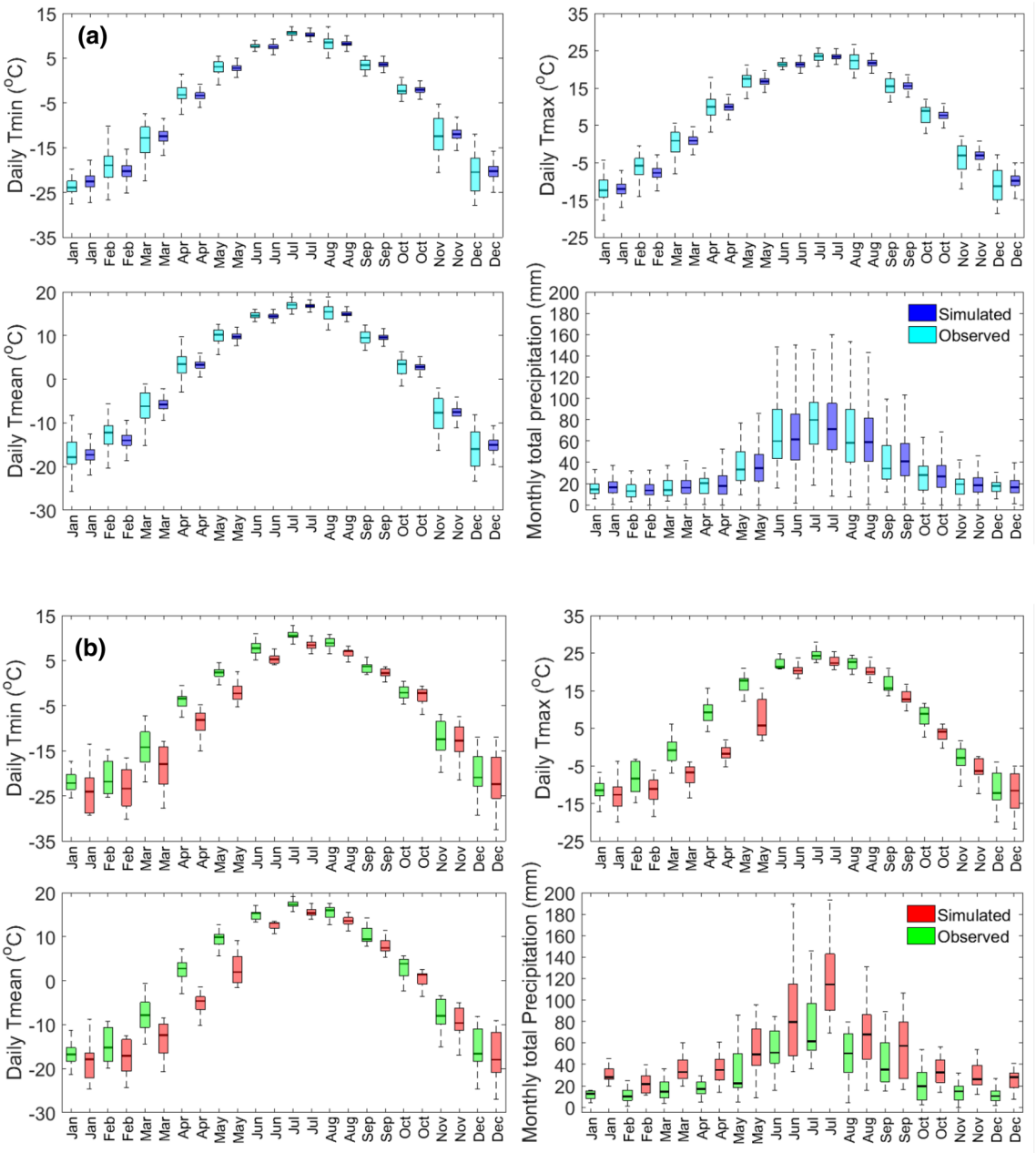

Fig. 2 Comparison between the month-wise temperature and precipitation for the observed ECCC time series, and the time series generated by **a** LARS-WG during the historical baseline period 1976–2005 and **b** WRF-CTL during the historical baseline period 2001–2015 at Fort McMurray Airport station. The boxplots represent the inter quartile range (IQR) values with median shown as black thick line, with whiskers showing values within 1.5 IQR extending from both ends of the boxes

as compared to the observations, are illustrative of the cold and wet biases of the WRF model. The simulated Tmin, Tmax, and Tmean in July were 8.43, 22.3, and 15.4 °C, respectively, while the observations were 10.5, 24.3, and 17.3 °C, respectively, and the median monthly precipitation in July was 115 mm for WRF, compared to the observed value of 61.5 mm.

These biases in temperature and precipitation would result in biases in the calculated PET and simulated water balance components, which are described in the following sections. Results with biases relative to the historical observed values will be used in the subsequent interpretations; therefore, the directions of change in the future water balance components relative to the baseline values from WRF simulations will be the basis of comparison with the LARS-WG simulations.

The observed annual median daily Tmin, Tmax, Tmean, and total precipitation are − 2.2, 9.1, and 3.6 °C,

and 421.1 mm, respectively, during the 1976–2005 time period and − 2.3, 9.0, and 3.2 °C, and 374.2 mm, respectively, during the 2001–2015 time period. The statistics associated with these two different historical time periods are not significantly different and consequently provide a valid comparison to the downscaled model projections. The median daily T_{min}, T_{max}, T_{mean}, and total precipitation from the LARS-WG projections were − 2.3, 9.0, and 3.4 °C, and 424.2 mm, respectively for 1976–2005. The WRF projections were − 4.7, 1.3, and − 1.4 °C, and 584.5 mm, respectively, for 2001–2015.

Comparison of LARS-WG and WRF in Future Periods

Changes in the monthly median temperature and precipitation from the baseline to future period predictions for the two downscaling methods are shown in Table 1. Overall, both models show increases in temperature and precipitation in nearly all months (the exceptions being June and September precipitation changes for WRF and the August changes in precipitation for LARS). The maximum temperature and precipitation for both models occurs in July with the minimum temperature and precipitation in February for both the baseline and future periods. Both models show a similar shift in all monthly temperatures from baseline to future time periods of ≈ 3.2–8.9 °C (average monthly change of 5.0 °C for LARS and 5.5 °C for WRF). They also show a consistent shift in monthly precipitation of ≈ 8.0 mm decrease to 22.9 mm increase (average monthly change of 3.4 mm for LARS and 5.8 mm for WRF). The increases in temperature in both the spring and fall highlight a potential increased growing season and a shorter winter period during which the snowpack might accumulate.

Both methods predict similar shifts in temperature and precipitation for most months with a decrease in precipitation in a few months (June, August, and September) during the growing season. The decrease in precipitation in some months might potentially affect water availability for vegetation growth in some years. However, increases in the spring and fall precipitation, when evapotranspiration demand might be quite low, can potentially lead to higher NP rates.

In general, the baseline and future temperature from WRF shows higher variability than those from LARS-WG. The average CV values for LARS-WG during baseline and future periods were 13.8% and 18.8%, respectively, while the corresponding CV values for WRF were 93.2% and 58.9%. In contrast, the baseline and future precipitation from LARS-WG shows greater variability than that predicted by WRF. The average CV values for LARS-WG during baseline and future periods were 52.3% and 53.6%, respectively, while the corresponding CV values for WRF were 42.3% and 40.8%. Supplemental Table S-2 shows the monthly CV values from the baseline to future period predictions for the two downscaling methods.

Since the LARS-WG predictions are based on adjusting the predicted precipitation probability distributions to the local scale observations, the impact of local scale convective precipitation events is implicitly reflected within these adjustments. Generally, GCMs are unable to represent the convective processes and are expected to show less variability than WRF, while both raw GCMs and WRF simulations are expected to show less variability than the site-specific LARS-WG simulations. In this way, extreme convective

Table 1 The median daily future T_{mean} and total precipitation during the baseline and future periods, and changes in median daily future T_{mean} and total precipitation relative to the corresponding baseline periods during each month for two downscaling methods

Month	LARS-WG						WRF					
	T_{mean} (°C)			Precipitation (mm)			T_{mean} (°C)			Precipitation (mm)		
	Baseline	Future	Change (°C)	Baseline	Future	Change (mm)	Baseline	Future	Change (°C)	Baseline	Future	Change (mm)
Jan	− 17.3	− 10.2	7.1	16.5	19.5	3.0	− 17.9	− 12.1	5.8	28.2	38.3	10.1
Feb	− 14.0	− 7.7	6.3	13.8	17.2	3.4	− 17.0	− 11.7	5.3	21.7	26.1	4.4
Mar	− 5.8	− 1.1	4.7	16.4	19.9	3.5	− 12.4	− 5.8	6.6	32.8	48.1	15.3
Apr	3.3	6.5	3.2	18.1	21.5	3.5	− 4.6	1.3	5.9	34.9	39.7	4.8
May	9.8	14.0	4.2	34.7	41.2	6.5	2.0	9.5	7.5	49.2	72.1	22.9
Jun	14.4	18.9	4.5	61.8	67.1	5.3	13.1	16.5	3.4	79.4	72.8	-6.6
Jul	16.8	21.8	5.0	71.8	78.7	6.9	15.4	19.0	3.6	114.5	114.9	0.4
Aug	15.0	20.4	5.4	59.6	55.1	-4.5	13.6	17.6	4.0	68.0	73.4	5.4
Sep	9.6	14.6	5.0	41.5	44.4	2.9	7.5	11.5	4.0	57.3	49.3	− 8.0
Oct	2.8	6.4	3.6	26.9	31.7	4.8	1.4	5.6	4.2	32.7	37.2	4.5
Nov	− 7.5	− 3.0	4.5	18.7	21.8	3.1	− 9.6	− 2.5	7.1	26.3	31.8	5.5
Dec	− 15.1	− 8.3	6.8	16.8	19.4	2.6	− 17.9	− 9.0	8.9	28.2	39.3	11.1
Overall	1.0	6.0	5.0	33.1	36.5	3.4	− 2.2	3.3	5.5	47.8	53.6	5.8

events are more realistically captured by LARS-WG or WRF than GCMs simulations. The calculated CV values for the future daily precipitation for raw GCMs, WRF, and LARS-WG were 213, 219, and 242%, respectively, while the maximum daily precipitation amounts simulated by the GCMs, WRF, and LARS-WG were 61, 101, and 101 mm, respectively. However, it should be kept in mind that the WRF results are affected by the inherited biases from the driving GCMs.

Both downscaling methods predict increased growing season precipitation and PET in the future (2086–2100), relative to their baseline (1976–2005 for LARS-WG and 2001–2015 for WRF), as shown in Fig. 3. The median growing season precipitation measured at the Fort McMurray Airport station was 387 and 362 mm during 1976–2005 and 2001–2015, respectively. These values were well estimated by LARS-WG (387 mm) but overestimated by WRF (523 mm) due to a wet bias in the WRF model inherited from the driving GCMs. The median growing season PET values estimated using the Hargreaves-Samani method for 1976–2005 and 2001–2015 were 638 and 653 mm, respectively. The LARS-WG simulation was able to replicate this PET value for the corresponding baseline period (638 mm); however, WRF (541 mm) underestimated the PET value due to a cold bias.

Despite these differences, the overall relative shift (magnitude and direction) from the baseline to the future period for both growing season precipitation and PET were similar for both models. For example, the increase in median growing season precipitation for LARS-WG was 22.7%, while WRF predicted an increase of 11.5%. The increase in median growing season PET was 19.6% for LARS-WG and 19.4% increase for WRF. The uncertainty associated with growing season precipitation was larger for LARS-WG than WRF, while the same associated with PET was larger for WRF than LARS-WG, as evident in the distribution of the corresponding boxplots (Fig. 3) and CV values (not shown).

A probability density function (PDF) of growing season daily precipitation events can be used to compare the individual models and associated observations in a manner that highlights extreme precipitation events (Fig. 4). The comparison periods are 1976–2005 for LARS-WG, and 2001–2015 for WRF. It is apparent that the WRF simulations overestimate the magnitude of precipitation events at all frequencies but increasingly so for high precipitation events. The LARS-WG simulations are consistent with the observed distribution, with the exception of the most extreme event.

Figure 4 also includes the distribution of daily growing season precipitation events for future periods: 2086–2100 for LARS-WG (Fig. 4a), and 2086–2100 for WRF (Fig. 4b). It is expected that an increase in extreme daily precipitation events would lead to increases in runoff. The differences in the shift of the PDF from the baseline to future predictions for the two models is quite striking. LARS-WG predicts a modest increase in daily precipitation at nearly all

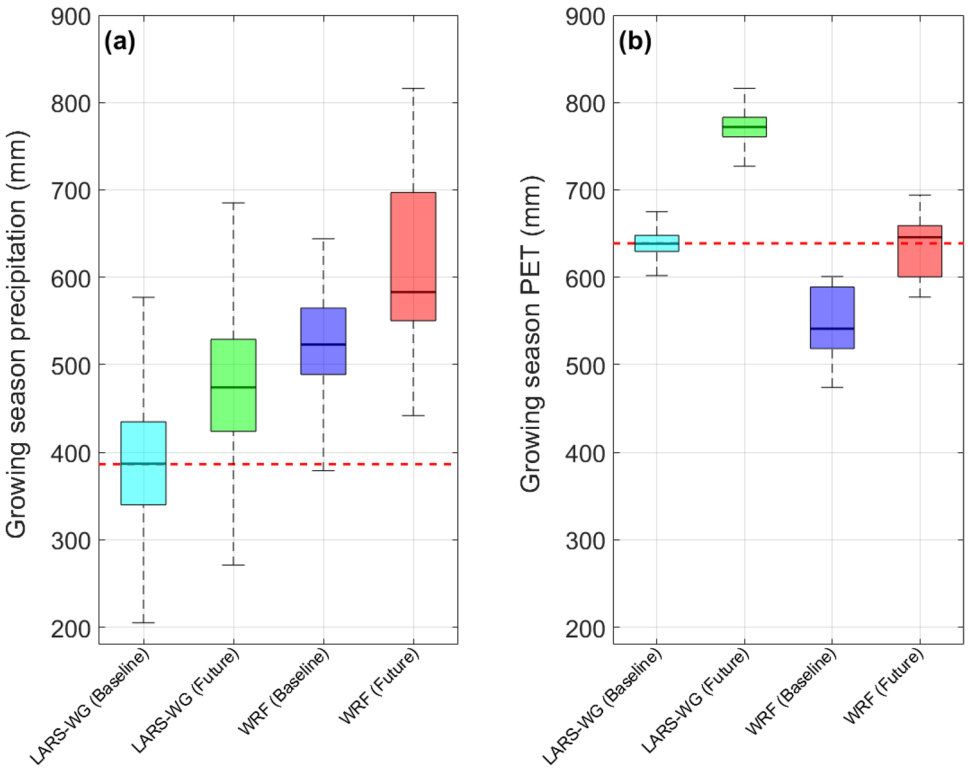

Fig. 3 Distributions of **a** growing season precipitation and **b** growing season PET based on 100 realizations from LARS-WG during baseline (1976–2005) and future (2086–2100) periods as well as based on WRF simulations for baseline (2001–2015) and future (2086–2100) periods at Fort McMurray Airport station. The horizontal dashed lines show median growing season precipitation and PET based on the observed monitoring data at Fort McMurray Airport station during 1976–2005. Description of boxplots is given in Fig. 2

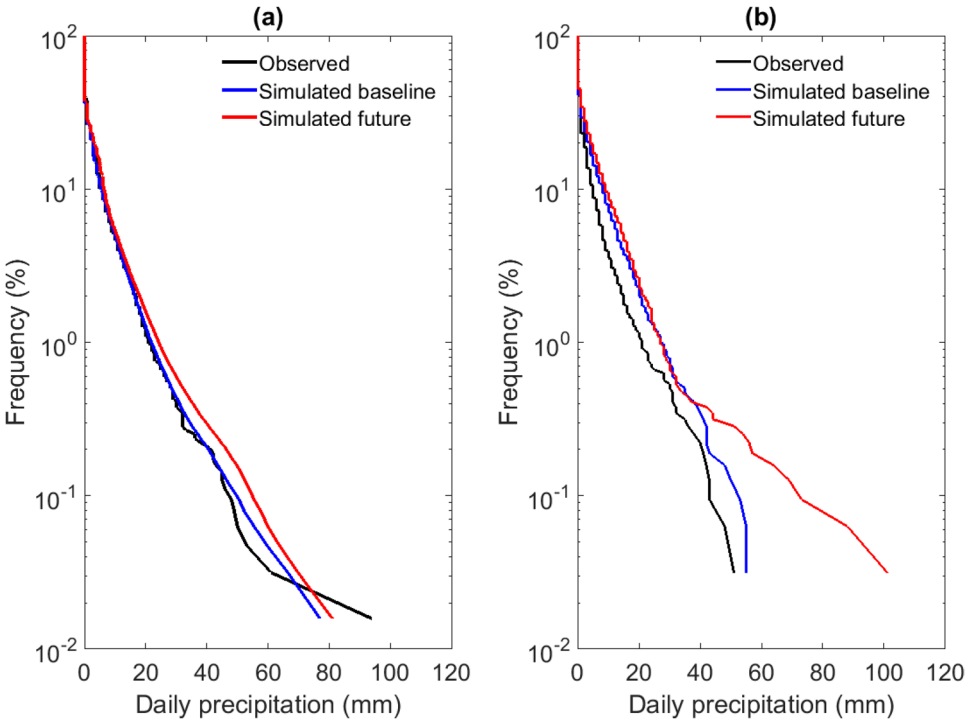

Fig. 4 Probability density function of daily precipitation during the growing season (i.e. April–October) at Fort McMurray Airport Station as **a** observed during 1976–2005, statistically downscaled by LARS-WG for the baseline (1976–2005) and future (2086–2100) periods and **b** observed during 2001–2015, dynamically downscaled by WRF for the baseline (2001–2015) and future (2086–2100) periods

frequencies, while the WRF predictions show similar magnitudes of precipitation events for both baseline and future predictions at frequencies greater than 0.5% but nearly double the magnitude of events in the future from the baseline at frequencies smaller than 0.05%. These more pronounced extreme events by WRF might be due to the overestimated distribution of baseline daily extreme precipitation relative to the historical observed amounts in the case of WRF. The shifted distribution of future daily extreme precipitation amounts relative to the baseline amounts demonstrates that these extreme precipitation events could be more prevalent in a changing climate condition.

Simulated Water Balance Components

The baseline historical climate projections for LARS-WG (1976–2005) and WRF (2001–2015) as well as the future projections (2086–2100) for both models were used as climatic inputs to the Hydrus water balance modeling of each of the three reclamation cover sites (D3, SWSS, and ACS) and the three natural soil profile sites (SV10, SV27, and SV60).

Figure 5 presents the simulated AET for the three reclamation covers and natural soil profiles. The AET for the reclamation covers are higher than for the natural soil profiles in all cases due to the finer texture of the reclamation covers (Alam et al. 2018). The magnitude and direction of change in the future median growing season AET, relative to the corresponding baseline AET using the two downscaling methods are similar for all of the study sites.

Figure 6 presents the simulated NP using the LARS-WG and WRF projections. All simulations show that NP is higher for the three natural soil profiles than the reclamation covers, as expected given their coarser texture (Alam et al. 2018). The direction of change in future NP, relative to the corresponding baseline NP are similar for both downscaling methods with similar directions of change in the future growing season NP for all of the study sites, although the shifts in future NP are greater for WRF than for LARS-WG.

The relative change in the simulated future AET relative to the baseline periods for the LARS-WG and WRF simulations are presented in Fig. 7. The median change in the future AET for both the WRF simulations and LARS-WG simulations are similar (boxes overlap in Fig. 7) to each other and similar for all cover types to the end of the twenty-first century. However, Fig. 7 also highlights that LARS-WG based simulations have a greater degree of variability in the projected changes in AET than the WRF simulations. WRF climate projections capture more variability in monthly temperatures, while LARS-WG capture more variability in monthly precipitation. The variability in future AET and corresponding % changes appear to be controlled by variability in future precipitation rather than variability in future PET, with the result that higher variability in future precipitation leads to higher variability in future AET.

This is also true for the occurrence of extreme high and low AET values. The prevalence of extreme AET events, in

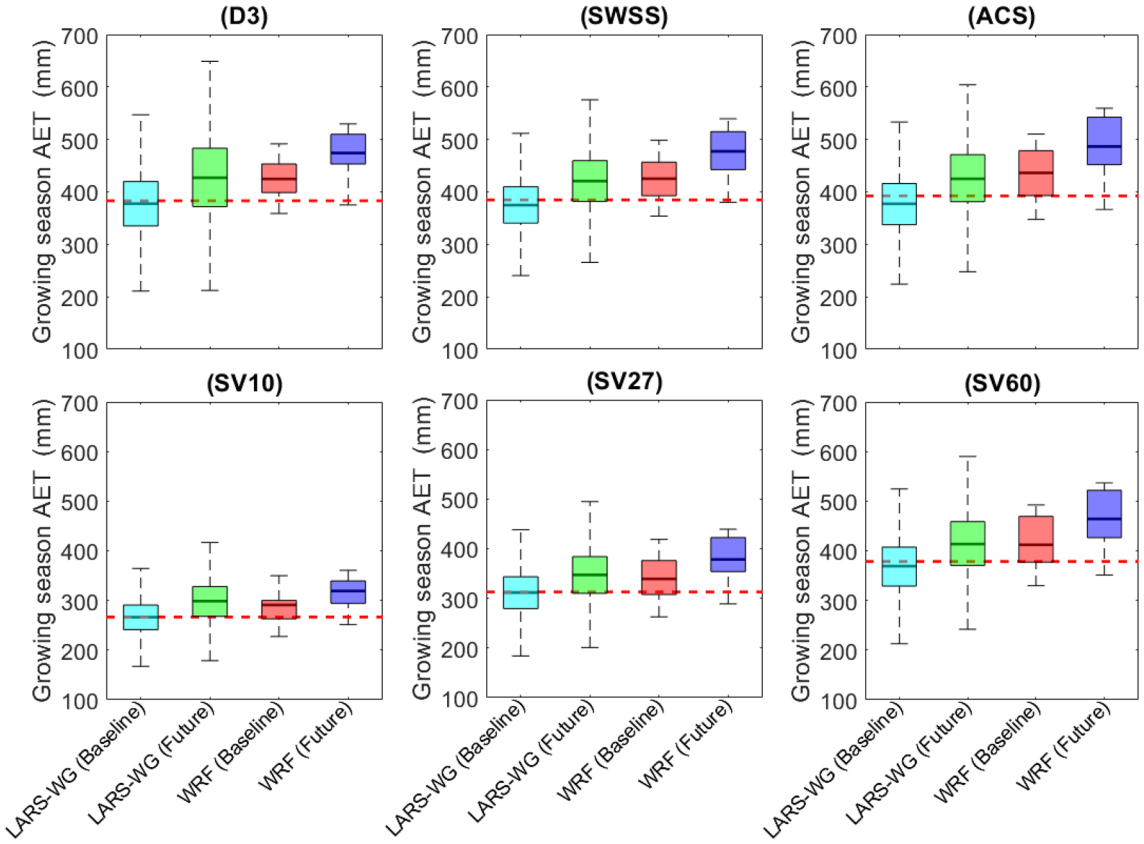

Fig. 5 Distributions of growing season AET for 100 realizations of climate change projections from LARS-WG during 1976–2005 (i.e. Baseline) and climate change projections from WRF during 2001–2015 (i.e. Baseline) as well as during 2086–2100 (i.e. Future). The results are shown for three reclamation covers (D3, SWSS, and ACS) and three natural soil profiles (SV10, SV27, and SV60). The horizontal dashed lines show median growing season AET based on the observed monitoring data at Fort McMurray Airport station during 1976–2005. Description of boxplots is given in Fig. 2

the case of LARS-WG, reflects more extremely wet or dry years toward the end of the twenty-first century compared to the WRF simulations. This would suggest a potential shift in optimal vegetation/tree selection for reclamation covers to adapt to more variability in AET, if LARS-WG simulations are used for reclamation cover design.

Figure 8 shows the percent change in the simulated future NP. The median % change in NP for both downscaling methods are once again similar (boxes overlap in Fig. 8); however, both LARS-WG and WRF show higher % changes in future NP for the reclamation covers (48–95%) than the three natural soil profiles (21–89%). Once again, the percentage change in NP exhibits more variability for the LARS-WG based simulations than for WRF, including a greater change in the percentage of extreme annual NP values.

Similar to the % changes in future AET, the variability in future NP appears to be controlled by the variability in future precipitation. The prevalence of extreme NP events, in the case of LARS-WG, reflects either more extreme wet or dry years toward the end of the twenty-first century compared to the WRF simulations. This might suggest that water yield from the reclaimed mine waste may be more variable if LARS-WG simulations are considered for the design of mine closure landscapes.

The relative magnitudes of the simulated precipitation for LARS-WG and WRF models seems to be reflected in the simulated water balance components (AET and NP) during the end of the twenty-first century. In particular, precipitation is the dominant climate variable in the predictions of the two key water balance components.

The range of the predicted changes in the future growing season AET and NP relative to the baseline periods is higher for LARS-WG than WRF, even though WRF predictions might be expected to capture more variability due to regional scale convective precipitation events. We mentioned earlier that LARS-WG showed higher variability in future precipitation than that shown by WRF and precipitation is the dominant variable in simulating AET and NP. It is important to note, however, that convective events generally last for only an hour in most cases. As a result, daily water balance modelling, as undertaken in this study, does not capture the potential impact of these events in triggering runoff events.

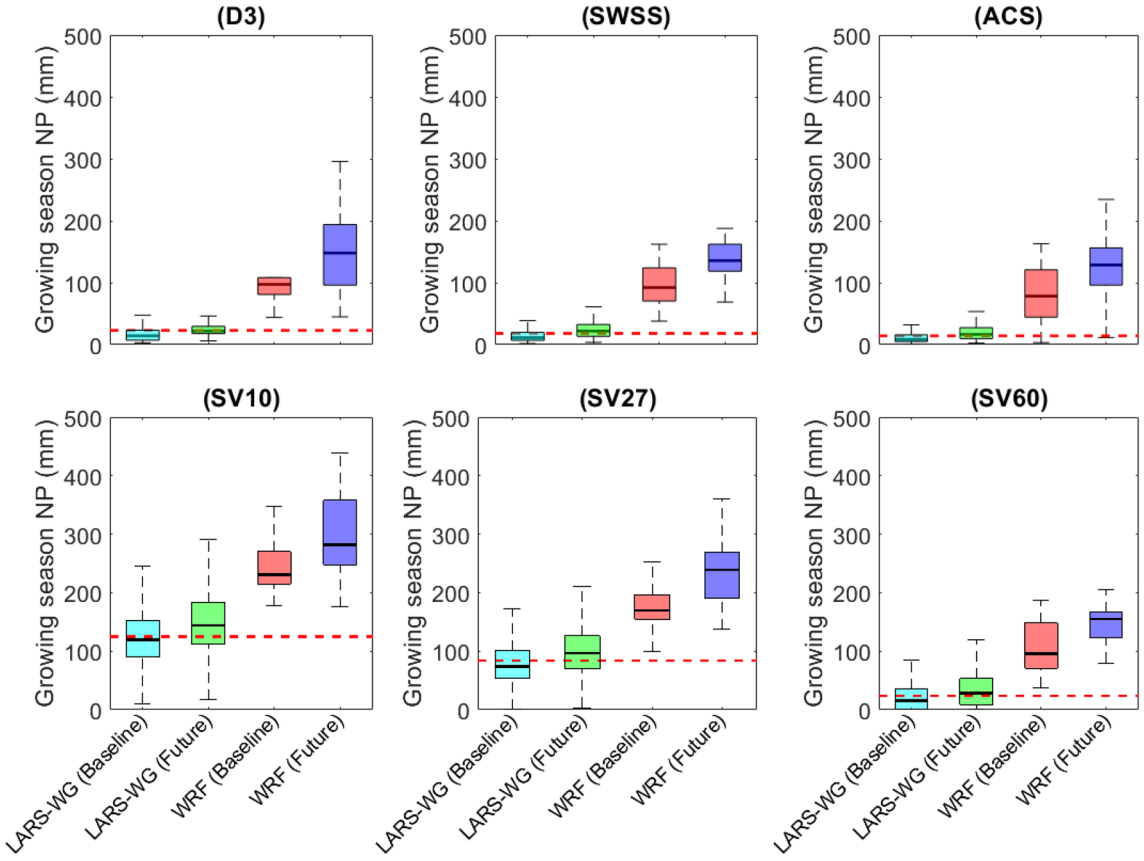

Fig. 6 Distributions of growing season NP for 100 realizations of climate change projections from LARS-WG during 1976–2005 (i.e. Baseline) and climate change projections from WRF during 2001–2015 (i.e. Baseline) as well as during 2086–2100 (i.e. Future). The results are shown for three reclamation covers (D3, SWSS, and ACS) and three natural soil profiles (SV10, SV27, and SV60). The horizontal dashed lines show median growing season NP based on the observed monitoring data at Fort McMurray Airport station during 1976–2005. Description of boxplots is given in Fig. 2

The impact of these convective events is further diminished when the results are accumulated into monthly and/or growing season amounts.

The key growing season water balance components (i.e. AET and NP) for all sites are summarized in Table 2. The median growing season AET values from LARS-WG for the baseline period were comparable to the values reported by Alam et al. (2018) for all sites, except ACS. This was despite the baseline periods being different (1976–2005 in this study and 1961–1990 in Alam et al. 2018). The baseline period AET of the ACS site was less (377 mm) than in the previous study (402 mm; Alam et al. 2020), due to the difference in the median growing season precipitation used in the model simulations for the two baseline periods (387 mm from 1976 to 2005 in this study; 407 mm from 1961 to 1990 for Alam et al. 2018), while Alam et al. (2020) used a value of 426 mm for the baseline period 1954–2013. Zhang et al. (2018) showed that the selection of baseline period is a likely source of uncertainty in studying the impacts of climate change.

The simulated growing season NP in this study are also different from those in the previous studies because of the differences in growing season precipitation from the different baseline periods, which in turn directly affect the growing season AET and NP values, as shown by LARS-WG simulations. Considering all sites, the increases in AET are ≈ 11.4–13.1% for LARS-WG and 9.6–12.6% for WRF, while the increases in NP are ≈ 20.8–95.0% for LARS-WG and 21.9–64.5% for WRF. In particular, reclamation covers and natural soil sites show a similar range of increase in AET; however, the percentage increases in NP are more pronounced for the reclamation covers than the natural sites. The increased future AET might be expected to produce a change in overall productivity of these sites but may also result in a shift in the vegetative regime that is established. The increased future NP could lead to increased water release from these reclaimed mine waste landforms with a concomitant increase in chemical loading due to flushing of these deposits by recharge waters.

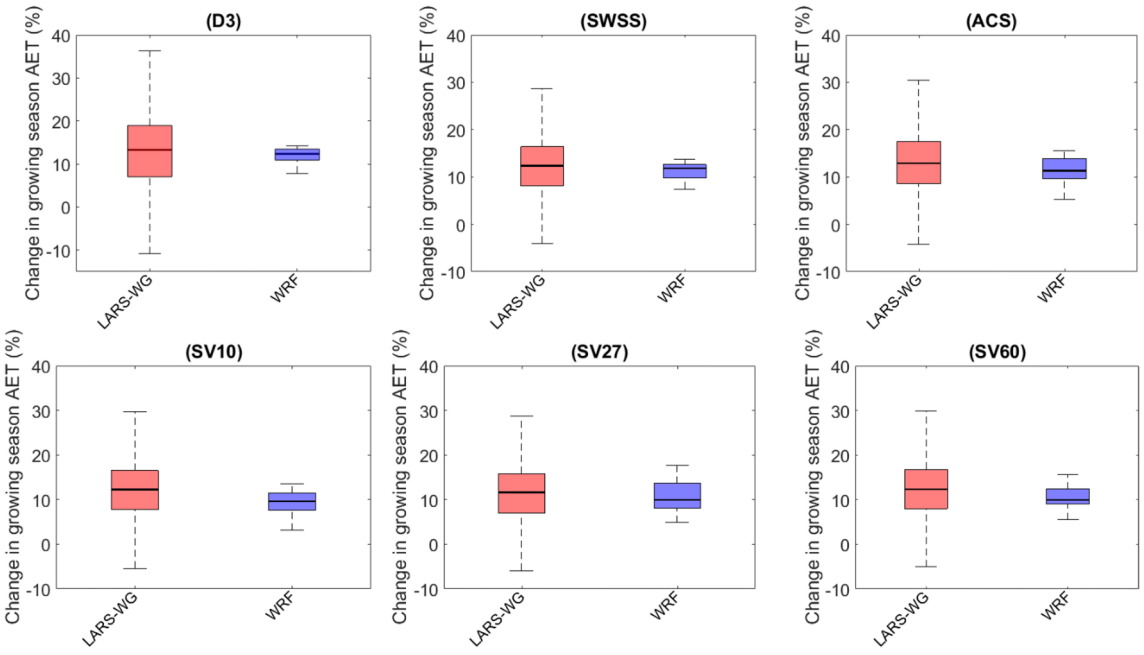

Fig. 7 Distributions of growing season AET based on an ensemble of 17 GCMs based on RCP8.5 from CMIP5 and downscaled by LARS-WG (red boxes) and based on the climate change projections downscaled by WRF (blue boxes) during the end of the twenty-first century. The results are shown for three reclamation covers (D3, SWSS, and ACS) and three natural soil profiles (SV10, SV27, and SV60). Description of boxplots is given in Fig. 2

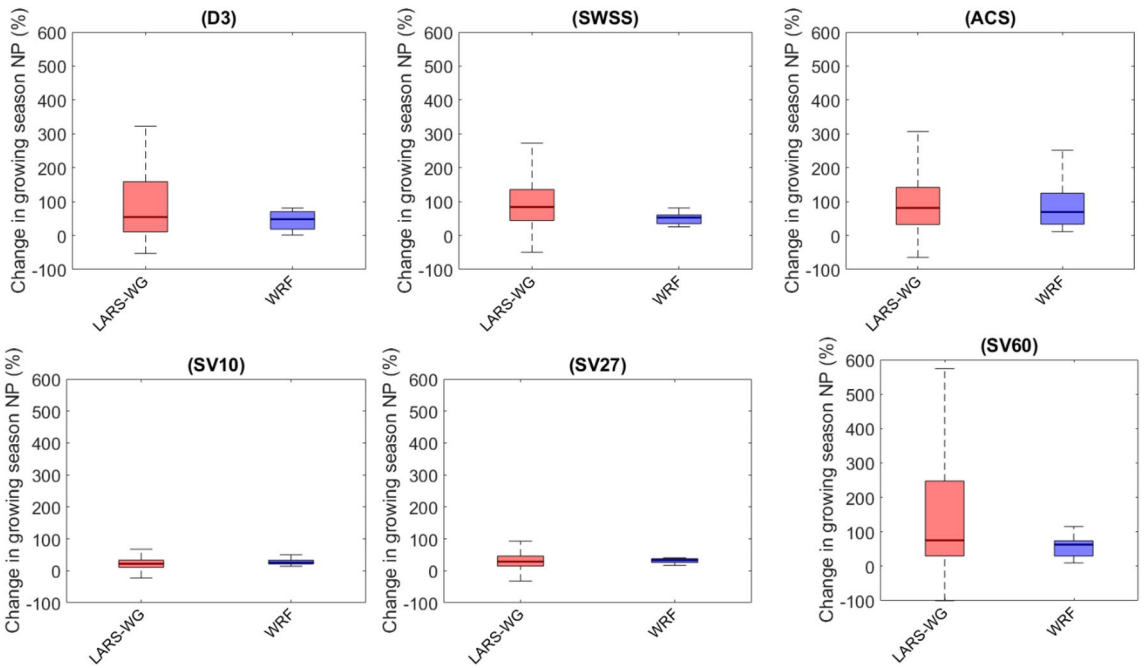

Fig. 8 Distributions of growing season NP based on an ensemble of 17 GCMs based on RCP8.5 from CMIP5 and downscaled by LARS-WG (red boxes) and based on the climate change projections downscaled by WRF (blue boxes) during the end of the twenty-first century. The results are shown for three reclamation covers (D3, SWSS, and ACS) and three natural soil profiles (SV10, SV27, and SV60). Description of boxplots is given in Fig. 2

Table 2 Growing season median precipitation, AET, and NP for the baseline and future periods based on the LARS-WG and WRF simulations

	Precipitation (mm)				AET (mm)				NP (mm)			
	LARS-WG		WRF		LARS-WG		WRF		LARS-WG		WRF	
	Baseline	Future	Baseline	Future	Baseline	Future	Baseline	Future	Baseline	Future	Baseline	Future
Site	(1976–2005)	(2086–2100)	(2001–2015)	(2086–2100)	(1976–2005)	(2086–2100)	(2001–2015)	(2086–2100)	(1976–2005)	(2086–2100)	(2001–2015)	(2086–2100)
D3	387	474 (22.7%)	523	583 (11.5%)	377	427 (13.1%)	425	474 (11.6%)	14.2	21.9 (53.9%)	97.3	148 (52.0%)
SWSS	387	474 (22.7%)	523	583 (11.5%)	375	421 (12.2%)	425	477 (12.2%)	11.2	21.9 (94.7%)	92.2	136 (47.2%)
ACS	387	474 (22.7%)	523	583 (11.5%)	377	425 (12.6%)	436	487 (11.5%)	8.5	16.5 (95.0%)	78.2	129 (64.5%)
SV10	387	474 (22.7%)	523	583 (11.5%)	266	299 (12.2%)	291	319 (9.6%)	119	144 (20.8%)	231	282 (21.9%)
SV27	387	474 (22.7%)	523	583 (11.5%)	312	347 (11.4%)	339	378 (11.6%)	74.3	96.6 (30.1%)	170	239 (40.7%)
SV60	387	474 (22.7%)	523	583 (11.5%)	369	414 (12.1%)	412	464 (12.6%)	15.1	28.5 (88.9%)	95.3	155 (62.8%)

The percentage increases in the future median precipitation, AET and NP relative to the baseline median precipitation, AET and NP are shown in parentheses

Conclusion

The impact of climate change projections on the long-term water balances of reclamation covers, as well as natural soil profiles, was evaluated using a physically-based water balance model and future climate change predictions from different downscaling methods. The use of both dynamical (WRF) and statistical (LARS-WG) downscaling methods provides a novel approach for comparing the long-term future performances of reclamation covers compared to those of natural soil profiles.

When comparing the simulated temperature and precipitation from the downscaling models to the observational data, it is clear that the statistical downscaling method (LARS-WG) outperformed the dynamical downscaling method (WRF). In most months, WRF predictions systematically underestimated temperature and overestimated precipitation. In addition, the computational demand for WRF simulations was much higher than that for LARS-WG. The directional shifts in the monthly future temperature and precipitation from the baseline periods were, however, similar for both downscaling methods. Both downscaling methods also showed similar directional shifts in the future median growing season AET and NP from the baseline periods.

The magnitude of increase in growing season median AET and NP using the WRF climate predictions were not significantly different from those using the LARS-WG climate predictions, although LARS-WG showed more variability in these water balance components. Overall, the increases (%) in future NP were significantly higher than increases (%) in future AET, particularly for the reclamation covers. LARS-WG based projections had more extreme (high and low) AET and NP values than the WRF model. Although the two downscaling methods are based on different approaches, both methods indicate similar relative changes in the growing season water balance components (i.e. AET and NP) by the end of the twenty-first century. Overall, the changes in the future key water balance components for LARS-WG show greater variability than those of the WRF model.

The systematic under- and over-estimation of temperature and precipitation, respectively, during the baseline period (2001–2015) by WRF was explained by Li et al. (2019) as being due to cold and wet biases, respectively. These biases are expected to carry into the future projections and the resulting future growing season water balance components. This allows the relative changes in the water balance components arising due to climate change to be evaluated, but not the absolute values. The WRF model would require bias correction to generate realistic absolute water balance components.

Both downscaling methods have advantages and limitations, although further comparisons for aligned modelling time frames will be required to guide policy makers and industry on how to best make reliable decisions on cover performance. It is likely that a multi-model approach (multiple GCM, RCPs, and downscaling methods) will be required to fully explore the potential impact of future climate changes on reclamation cover performance and ultimately on mine closure strategies.

Since the LARS-WG and WRF showed similar directions of shifts in the future water balance components from the baseline periods using an ensemble of GCMs from CMIP5, future extensions of this study will re-evaluate the shifts in future water balance components from LARS-WG and WRF using the newly released ensemble of GCMs from CMIP6. The CMIP6 includes more GCMs and newly developed socio-economic emission scenarios (Eyring et al. 2016). Further evaluation will be expanded to the full range of reclamation covers and mine waste types currently being used by the oil sands industry (e.g. reclamation covers over overburden, lean oil sands, coke, and treated fine tailings). The relative contributions of spatial and temporal variability in the soil hydraulic properties and future climate variability to the total variability in the water balance components will be investigated using the full range of reclamation covers being monitored over many years and climate change projections from the downscaling methods.

Acknowledgements The work was financed by the Natural Sciences and Engineering Research Council of Canada (NSERC) and Syncrude Canada Ltd. (File No. IRCPJ 428588-11; IRCSA 428587-11). Special thanks to (a) Dr. Zhenhua Li for sharing the WRF model outputs, and (b) Amy Heidman of O'Kane Consultants Inc. for providing uninterrupted access to the Syncrude watershed research database. We thank Stephanie Villeneuve for preparing Fig. 1.

Data and Material Availability Climate and soil monitoring data for all the reclamation covers at the Mildred Lake and Aurora North mine sites are available through the Syncrude watershed research database (https://syncrude.emline.ca/) per the outlined data policy. The global climate model outputs are made available by the WCRP (https://esgf-node.llnl.gov/). For the WRF results, please contact the co-author, Dr. Yanping Li. For all other data, simulated water balance components, and code required to run Hydrus-1D, please contact the corresponding author.

References

Alam MS, Barbour SL, Elshorbagy A, Huang M (2018) The impact of climate change on the water balance of oil sands reclamation covers and natural soil profiles. J Hydrometeorol 19:1731–1752. https://doi.org/10.1175/JHM-D-17-0230.1

Alam MS, Barbour SL, Huang M (2020) Characterizing uncertainty in the hydraulic parameters of oil sands mine reclamation covers and its influence on water balance predictions. Hydrol Earth Syst Sci 24:735–759. https://doi.org/10.5194/hess-24-735-2020

Alam MS, Elshorbagy A (2015) Quantification of the climate change-induced variations in intensity-duration-frequency curves in the Canadian prairies. J Hydrol 527:990–1005. https://doi.org/10.1016/j.jhydrol.2015.05.059

Alam MS, Barbour SL, Elshorbagy A, Huang M (2017) The impact of climate change on the performance of oil sands reclamation covers: a comparison of multiple general circulation models and representative concentration pathways. In: Proceedings of 70th Canadian Geotechnical Soc Conference, Ottawa

Alexander LV, Zhang X, Peterson TC, Caesar J, Gleason B, Klein Tank AMG, Haylock M, Collins D, Trewin B, Rahimzadeh F, Tagipour A, Rupa Kumar K, Revadekar J, Griffiths G, Vincent L, Stephenson DB, Burn J, Aguilar E, Brunet M, Taylor M, New M, Zhai P, Rusticucci M, Vazquez-Aguirre JL (2006) Global observed changes in daily climate extremes of temperature and precipitation. J Geophys Res 111:1–22. https://doi.org/10.1029/2005JD006290

Barbour SL, Chapman D, Qualizza C, Kessler S, Boese C, Shurniak R, Meiers M, O'Kane M, Wall S (2004) Tracking the evolution of reclaimed landscapes through the use of instrumented watersheds—a brief history of the Syncrude southwest 30 overburden reclamation research program. In: Proceedings of International Instrumented Watershed Symposium, Edmonton

Bockstette J (2018) The role of soil reconstruction and soil amendments in forest reclamation. MSc thesis, Department of Renewable Resources, University of Alberta

Boese CD (2003) The design and installation of a field instrumentation program for the evaluation of soil-atmosphere water fluxes in a vegetated cover over saline/sodic shale overburden. MSc thesis, University of Saskatchewan.

CAPP (Canadian Assoc of Petroleum Producers) (2019) Crude oil forecast, markets and transportation [online]. Available at https://www.capp.ca/resources/reports/. Accessed: 10 Jan 2020

CEMA (Cumulative Environmental Management Assoc) (2006) Land capability classification system for forest ecosystems in the oil sands, 3rd edit, vol 1: Field manual for land capability determination. Alberta Environment.

Carrera-Hernandez JJ, Mendoza CA, Devito KJ, Petrone RM, Smerdon BD (2011) Effects of aspen harvesting on groundwater recharge and water table dynamics in a subhumid climate. Water Resour Res 47(5):1–18. https://doi.org/10.1029/2010WR009684

Castro CL, Pielke RA, Leoncini G (2005) Dynamic downscaling: assessment of value retained and added using the regional atmospheric modeling system (RAMS). J Geophys Res 110:1–21. https://doi.org/10.1029/2004JD004721

Chen H (2013) Projected change in extreme rainfall events in China by the end of the 21st century using CMIP5 models. Chin Sci Bull 58(12):1462–1472. https://doi.org/10.1007/s11434-012-5612-2

Chun KP, Wheater HS, Nazemi A, Khaliq MN (2013) Precipitation downscaling in Canadian prairie provinces using the LARS-WG and GLM approaches. Can Water Resour J 38(4):311–332. https://doi.org/10.1080/07011784.2013.830368

Dee DP, Uppala SM, Simmons AJ, Berrisford P, Poli P, Kobayashi S, Andrae U, Balmaseda MA, Balsamo G, Bauer P, Bechtold P, Beljaars ACM, van de Berg L, Bidlot J, Bormann N, Delsol C, Dragani R, Fuentes M, Geer AJ, Haimberger L, Healy SB, Hersbach H, Holm EV, Isaksen L, Kallberg P, Kohler M, Matricardi M, McNally AP, Monge-Sanz BM, Morcrette JJ, Park BK, Peubey C, de Rosnay P, Tavolato C, Thepaut JN, Vitart F (2011) The ERA-Interim reanalysis: configuration and performance of the data assimilation system. Q J R Meteorol Soc 137(656):553–597. https://doi.org/10.1002/qj.828

Dobchuk BS, Shurniak RE, Barbour SL, O'Kane MA, Song Q (2013) Long-term monitoring and modelling of a reclaimed watershed cover on oil sands tailings. Int J Min Reclam Env 27(3):180–201. https://doi.org/10.1080/17480930.2012.679477

Done J, Davis CA, Weisman M (2004) The next generation of NWP: explicit forecasts of convection using the weather research and forecasting (WRF) model. Atmos Sci Lett 5(6):110–117. https://doi.org/10.1002/asl.72

Eyring V, Bony S, Meehl GA, Senior CA, Stevens B, Stouffer RJ, Taylor KE (2016) Overview of the coupled model intercomparison project phase 6 (CMIP6) experimental design and organization. Geosci Model Dev 9:1937–1958. https://doi.org/10.5194/gmd-9-1937-2016

Feddes RA, Bresler E, Neuman SP (1974) Field test of a modified numerical model for water uptake by root systems. Water Resour Res 10:1199–1206. https://doi.org/10.1029/WR010i006p01199

Foley AM (2010) Uncertainty in regional climate modelling: a review. Prog Phys Geogr 34:647–670. https://doi.org/10.1177/0309133310375654

Fosser G, Khodayar S, Berg P (2015) Benefit of convection permitting climate model simulations in the representation of convective precipitation. Clim Dyn 44(1–2):45–60. https://doi.org/10.1007/s00382-014-2242-1

Fowler HJ, Blenkinsop S, Tebaldi C (2007) Linking climate change modelling to impacts studies: recent advances in downscaling techniques for hydrological. Int J Climatol 27:1547–1578. https://doi.org/10.1002/joc

Gao Y, Fu JS, Drake JB, Liu Y, Lamarque JF (2012) Projected changes of extreme weather events in the eastern United States based on a high resolution climate modeling system. Environ Res Lett 7(4):1–12. https://doi.org/10.1088/1748-9326/7/4/044025

Government of Alberta (2017) Oil sands: facts and stats. open.alberta.ca/publications/oil-sands-facts-and-stats, accessed 01 Jun 2020

Hargreaves GH, Samani ZA (1985) Reference crop evapotranspiration from temperature. Appl Eng Agric 1(2):96–99

Hassanzadeh E, Nazemi A, Elshorbagy A (2014) Quantile-based downscaling of precipitation using genetic programming: application to IDF curves in Saskatoon. J Hydrol Eng 19(5):943–955. https://doi.org/10.1061/(ASCE)HE.1943-5584.0000854

Held IM, Soden BJ (2006) Robust responses of the hydrological cycle to global warming. J Clim 19(21):5686–5699. https://doi.org/10.1175/JCLI3990.1

Huang M, Barbour SL, Carey SK (2015a) The impact of reclamation cover depth on the performance of reclaimed shale overburden at an oil sands mine in northern Alberta, Canada. Hydrol Process 29(12):2840–2854. https://doi.org/10.1002/hyp.10229

Huang M, Elshorbagy A, Lee Barbour S, Zettl J, Si BC (2011a) System dynamics modeling of infiltration and drainage in layered coarse soil. Can J Soil Sci 91(2):185–197. https://doi.org/10.4141/cjss10009

Huang M, Hilderman JN, Barbour SL (2015b) Transport of stable isotopes of water and sulphate within reclaimed oil sands saline-sodic mine overburden. J Hydrol 529:1550–1561. https://doi.org/10.1016/j.jhydrol.2015.08.028

Huang M, Lee Barbour S, Elshorbagy A, Zettl J, Si BC (2011b) Water availability and forest growth in coarse-textured soils. Can J Soil Sci 91(2):199–210. https://doi.org/10.4141/cjss10012

Huang M, Lee Barbour S, Elshorbagy A, Zettl JD, Si BC (2011c) Infiltration and drainage processes in multi-layered coarse soils. Can J Soil Sci 91(2):169–183. https://doi.org/10.4141/cjss09118

IPCC Intergovernmental Panel on Climate Change (2000) Land use, land-use change and forestry: a special report of the IPCC. Watson R, Noble I, Bolin B, Ravindranath NH, Verardo D, Andrasko K (Eds), Cambridge University Press, Cambridge

IPCC Intergovernmental Panel on Climate Change (2013) Climate Change 2013: The Physical Science Basis. In: Stocker QD (ed) Contribution of Working Group I to the 5th Assessment Report of the Intergovernmental Panel on Climate Change. Cambridge University Press, Cambridge

Joubert AM, Hewitson BC (1997) Simulating present and future climates of southern Africa using general circulation models. Prog Phys Geogr 21(1):51–78. https://doi.org/10.1177/030913339702100104

Karl TR, Knight RW, Plummer N (1995) Trends in high-frequency climate variability in the twentieth century. Nature 377(6546):217–220. https://doi.org/10.1038/377217a0

Keshta N, Elshorbagy A, Carey S (2009) A generic system dynamics model for simulating and evaluating the hydrological performance of reconstructed watersheds. Hydrol Earth Syst Sci 13(6):865–881. https://doi.org/10.5194/hess-13-865-2009

Keshta N, Elshorbagy A, Carey S (2012) Impacts of climate change on soil moisture and evapotranspiration in reconstructed watersheds in northern Alberta Canada. Hydrol Process 26(9):1321–1331. https://doi.org/10.1002/hyp.8215

Li Y, Li Z, Zhang Z, Chen L, Kurkute S, Scaff L, Pan X (2019) High-resolution regional climate modeling and projection over western Canada using a weather research forecasting model with a pseudo-global warming approach. Hydrol Earth Syst Sci 23(11):4635–4659. https://doi.org/10.5194/hess-23-4635-2019

Li Y, Szeto K, Stewart RE, Thériault JM, Chen L, Kochtubajda B, Liu A, Boodoo S, Goodson R, Mooney C, Kurkute S (2017) A numerical study of the June 2013 flood-producing extreme rainstorm over southern Alberta. J Hydrometeorol 18(8):2057–2078. https://doi.org/10.1175/JHM-D-15-0176.1

Liu C, Ikeda K, Rasmussen R, Barlage M, Newman AJ, Prein AF, Chen F, Chen L, Clark M, Dai A, Dudhia J, Eidhammer T, Gochis D, Gutmann E, Kurkute S, Li Y, Thompson G, Yates D (2017) Continental-scale convection-permitting modeling of the current and future climate of North America. Clim Dyn 49(1–2):71–95. https://doi.org/10.1007/s00382-016-3327-9

May W (2008) Potential future changes in the characteristics of daily precipitation in Europe simulated by the HIRHAM regional climate model. Clim Dyn 30(6):581–603. https://doi.org/10.1007/s00382-007-0309-y

Meehl GA, Covey C, Delworth T, Latif M, McAvaney B, Mitchell JFB, Stouffer RJ, Taylor KE (2007) The WCRP CMIP3 multimodel dataset: a new era in climate change research. Bull Am Meteorol Soc 88(9):1383–1394. https://doi.org/10.1175/BAMS-88-9-1383

Meehl GA, Covey C, Mcavaney B, Latif M, Stouffer RJ (2004) Overview of the coupled model intercomparison project. Bull Am Meteorol Soc 86(1):89–96. https://doi.org/10.1175/BAMS-86-1-89

Meiers GP, Barbour SL, Qualizza CV, Dobchuk BS (2011) Evolution of the hydraulic conductivity of reclamation covers over sodic/saline mining overburden. J Geotech Geoenviron 137(10):968–976. https://doi.org/10.1061/(ASCE)GT.1943-5606.0000523

Mitchell TD, Hulme M (1999) Predicting regional climate change: living with uncertainty. Prog Phys Geogr 23:57–78. https://doi.org/10.1191/030913399672023346

Nazemi A, Elshorbagy A, Pingale S (2011) Uncertainties in the estimation of future annual extreme daily rainfall for the city of Saskatoon under climate change effects. In: Proceedings of 20th Canadian Hydrotechnical Conf, Ottawa

OKC (O'Kane Consultants Inc) (2001) Southwest sand storage and 30-dump automated water balance monitoring systems at Syncrude Canada Ltd, OKC Report 653–2

OKC (O'Kane Consultants Inc) (2016) Instrumented watershed monitoring program at the southwest sands storage facility: Performance monitoring report for the period Jan 2015 to Dec 2015. OKC Report 690-01-72

Prein AF, Rasmussen RM, Ikeda K, Liu C, Clark MP, Holland GJ (2017) The future intensification of hourly precipitation extremes. Nat Clim Change 7(1):48–52. https://doi.org/10.1038/nclimate3168

Price JS, McLaren RG, Rudolph DL (2010) Landscape restoration after oil sands mining: conceptual design and hydrological modelling for fen reconstruction. Int J Min Reclam Environ 24(2):109–123. https://doi.org/10.1080/17480930902955724

Qualizza C, Chapman D, Barbour SL, Purdy B (2004) Reclamation research at Syncrude Canada's mining operation in Alberta's Athabasca oil sands region. In: Proceedings of 16th International Conf on Ecological Restoration SER2004, Victoria

Racsko P, Szeidl L, Semenov M (1991) A serial approach to local stochastic weather models. Ecol Model 57(1–2):27–41. https://doi.org/10.1016/0304-3800(91)90053-4

Rasmussen R, Ikeda K, Liu C, Gochis D, Clark M, Dai A, Gutmann E, Dudhia J, Chen F, Barlage M, Yates D, Zhang G (2014) Climate change impacts on the water balance of the Colorado headwaters: high-resolution regional climate model simulations. J Hydrometeorol 15(3):1091–1116. https://doi.org/10.1175/JHM-D-13-0118.1

Rasmussen R, Liu C, Ikeda K, Gochis D, Yates D, Chen F, Tewari M, Barlage M, Dudhia J, Yu W, Miller K, Arsenault K, Grubisic V, Thompson G, Gutmann E (2011) High-resolution coupled climate runoff simulations of seasonal snowfall over Colorado: a process study of current and warmer climate. J Clim 24(12):3015–3048. https://doi.org/10.1175/2010JCLI3985.1

Semenov MA (2007) Development of high-resolution UKCIP02-based climate change scenarios in the UK. Agric For Meteorol 144(1–2):127–138. https://doi.org/10.1016/j.agrformet.2007.02.003

Semenov MA, Barrow EM (1997) Use of a stochastic weather generator in the development of climate change scenarios. Clim Change 35(4):397–414. https://doi.org/10.1023/A:1005342632279

Sigouin MJP, Dyck M, Si BC, Hu W (2016) Monitoring soil water content at a heterogeneous oil sand reclamation site using a cosmic-ray soil moisture probe. J Hydrol 543(Part B):510–522. https://doi.org/10.1016/j.jhydrol.2016.10.026

Simunek J, Sejna M, Saito H, Sakai M, van Genuchten MT (2013) The HYDRUS software package for simulating the two- and three-dimensional movement of water, heat, and multiple solutes in variably-saturated media, Technical manual version 2.0, University of California, Riverside, CA

Skamarock C, Klemp B, Dudhia J, Gill O, Barker D, Duda G, Huang X, Wang W, Powers G (2008) A description of the advanced research WRF version 3. NCAR Technical Note NCAR/TN-475+STR. https://doi.org/10.5065/D68S4MVH

Srivastav RK, Schardong A, Simonovic SP (2014) Equidistance quantile matching method for updating IDF curves under climate change. Water Resour Manag 28(9):2539–2562. https://doi.org/10.1007/s11269-014-0626-y

Strong WL, Leggat KR (1981) Ecoregions of Alberta. Alberta Energy and Natural Resources Tech. Report T/4

Sun J (2014) Record-breaking SST over mid-North Atlantic and extreme high temperature over the Jianghuai–Jiangnan region of China in 2013. Chin Sci Bull 59(27):3465–3470. https://doi.org/10.1007/s11434-014-0425-0

Suncor Energy Inc. (2007) Climate change in the oil sands region. Voyager South Project Environmental Impact Report, Appendix 3, Government of Alberta. www.open.alberta.ca/publications/4070009. Accessed 01 Jun 2020

Taylor KE, Stouffer RJ, Meehl GA (2012) An overview of CMIP5 and the experiment design. Bull Am Meteorol Soc 93(4):485–498. https://doi.org/10.1175/BAMS-D-11-00094.1

Thompson C, Mendoza CA, Devito KJ (2017) Potential influence of climate change on ecosystems within the Boreal Plains of Alberta. Hydrol Process 31(11):2110–2124. https://doi.org/10.1002/hyp.11183

Weisman ML, Davis C, Wang W, Manning KW, Klemp JB, Weisman ML, Davis C, Wang W, Manning KW, Klemp JB (2008) Experiences with 0–36-h explicit convective forecasts with the WRF-ARW model. Weather Forecast 23(3):407–437. https://doi.org/10.1175/2007WAF2007005.1

Wilby RL, Wigley TML (1997) Downscaling general circulation model output: a review of methods and limitations. Prog Phys Geogr 21(4):530–548. https://doi.org/10.1177/030913339702100403

Wilby RL, Wigley TML, Conway D, Jones PD, Hewitson BC, Main J, Wilks DS (1998) Statistical downscaling of general circulation model output: a comparison of methods. Water Resour Res 34:2995–3008. https://doi.org/10.1029/98WR02577

Wilby RL, Dawson CW (2007) SDSM 4.2—a decision support tool for the assessment of regional climate change impacts: version 4.2, User Manual, Lancaster University, UK

Wood AW, Lettenmaier DP, Palmer RN (1997) Assessing climate change implications for water resources planning. Clim Change 37:203–228. https://doi.org/10.1007/978-94-017-1051-0_12

Zettl J, Lee Barbour S, Huang M, Si BC, Leskiw LA (2011) Influence of textural layering on field capacity of coarse soils. Can J Soil Sci 91(2):133–147. https://doi.org/10.4141/cjss09117

Zhang L, Nan Z, Yu W, Zhao Y, Xu Y (2018) Comparison of baseline period choices for separating climate and land use/land cover change impacts on watershed hydrology using distributed hydrological models. Sci Total Environ 622–623:1016–1028. https://doi.org/10.1016/j.scitotenv.2017.12.055

Zhang X, Vincent LA, Hogg W, Niitsoo A (2000) Temperature and precipitation trends in Canada during the 20th century. Atmos Ocean 38(3):395–429. https://doi.org/10.1080/07055900.2000.9649654